

Grain Boundary Transitions in Binary Alloys

Ming Tang and W. Craig Carter

Department of Materials Science and Engineering, Massachusetts Institute of Technology, Cambridge, Massachusetts 02139, USA

Rowland M. Cannon*

Lawrence Berkeley National Laboratory, Berkeley, California 94720, USA

(Received 19 May 2006; published 14 August 2006)

A thermodynamic diffuse interface analysis predicts that grain boundary transitions in solute absorption are coupled to localized structural order-disorder transitions. An example calculation of a planar grain boundary using a symmetric binary alloy shows that first-order boundary transitions can be predicted as a function of the crystallographic grain boundary misorientation and empirical gradient coefficients. The predictions are compared to published experimental observations.

DOI: 10.1103/PhysRevLett.97.075502

PACS numbers: 61.72.Bb, 61.72.Mm, 68.35.Rh

A grain boundary (GB) is an interface that separates the two orientations of abutting crystals of the same bulk phase. Many material properties depend on the transmission of forces and fields across a grain boundary and can be sensitive to grain boundary structure, chemistry, and morphology. At equilibrium, a GB's structure (the atomic configuration that produces the misorientation \mathcal{R}), morphology (the interface shape characterized by local interface inclination \hat{n}), and chemistry (the interfacial excess Γ_i of each independent chemical component species) are determined by the minimum of excess energy $\gamma_{\text{GB}}(T, P, \vec{\mu}; \mathcal{R}, \langle \hat{n} \rangle)$ when the abutting crystals are in equilibrium with the same pressure, temperature and chemical potentials $\vec{\mu} = (\mu_1, \mu_2, \dots, \mu_C)$ [1]. Grain boundary transitions occur if a different boundary structure, chemistry, or morphology has a reduced γ_{GB} . These transitions can be cooperative, such as segregation induced GB structural transitions [2].

Grain boundary transitions will produce abrupt changes in boundary-sensitive properties. If a sufficiently large fraction of grain boundaries in a polycrystal transform over a small range of temperatures or $\vec{\mu}$, macroscopic properties can undergo significant alteration. Examples include diffusivity, plasticity, conductivity, corrosion resistance, brittle-ductile transitions, and activated sintering [3,4].

The existence of GB premelting (onset of localized subsolidus or subeutectic structural disorder) was suggested as early as 1952 [5] and has been investigated numerically (lattice models [6], molecular dynamics [7], and Monte Carlo simulations [8]). While indirect observations support the existence of GB premelting [9], direct experimental observation in pure systems is rare [10]. In alloys, observations of GB structural disordering are less rare (reported for metals [11,12] and ceramics [4,13]) and are usually accompanied by changes in equilibrium GB

segregation. Models that treat simultaneous GB premelting and segregation are rare and system specific [6,12]. In this Letter, we present a generalized diffuse interface thermodynamic model for cooperative structural and chemical grain boundary transitions in binary alloys.

Using a diffuse interface GB model [14], we produced an analysis of GB structural transitions in fixed stoichiometry polycrystals [15], and it is extended to spatially variable compositions below. The total free energy of a planar GB is modeled as a functional of three fields: the composition, crystallinity (characterizing structural disorder), and crystallographic orientation, $c(x)$, $\eta(x)$, $\theta(x)$ [16]:

$$F[c, \eta, \theta; T] = \int_L \left[\Delta f(c, \eta; T) + \frac{\kappa^2}{2} \left(\frac{dc}{dx} \right)^2 + \frac{\nu^2}{2} \left(\frac{d\eta}{dx} \right)^2 + sg(\eta) \left| \frac{d\theta}{dx} \right| \right] dx, \quad (1)$$

where Δf is the excess free energy density with respect to the perfectly crystalline state ($\eta = 1$) at a fixed bulk composition c_∞ : $\Delta f = f(c, \eta; T) - f(c_\infty, \eta = 1; T) - \partial f / \partial c(c_\infty, \eta = 1; T)(c - c_\infty)$ [18]; the c -, η -, and θ -gradient coefficients ($\kappa^2/2$, $\nu^2/2$, and s) are treated as constants in this model. The coupling between the orientation gradient and η is assumed to be $g(\eta) = \eta^2$ [19].

The following boundary conditions model a solitary grain boundary within a single phase of a binary alloy: $c(x = \pm\infty) = c_\infty$, $\eta(x = \pm\infty) = 1$, and $\theta(x = \pm\infty) = \theta_\pm$. Assuming that $\eta(x)$ has only one local minimum at the GB core located at $x = 0$, it was shown [20] that, at equilibrium, $\theta(x)$ concentrates all its change at the GB center: $\theta^{\text{eq}}(x) = \theta_- + \Delta\theta H(x)$, where $H(x)$ is the unit step function and $\Delta\theta \equiv \theta_+ - \theta_-$. Substituting $\theta^{\text{eq}}(x)$ [i.e., $d\theta^{\text{eq}}/dx = \Delta\theta\delta(x)$] into Eq. (1) ($\Delta\theta > 0$ is assumed here),

$$F[c(x), \eta(x), \theta^{\text{eq}}; T; \eta_{\text{GB}}] = s\Delta\theta g(\eta_{\text{GB}}) + 2 \int_0^{+\infty} \left[\Delta f(c, \eta; T) + \frac{\kappa^2}{2} \left(\frac{dc}{dx} \right)^2 + \frac{\nu^2}{2} \left(\frac{d\eta}{dx} \right)^2 \right] dx, \quad (2)$$

where $\eta_{\text{GB}} \equiv \eta(x = 0)$ will characterize the maximum structural disorder at the GB core.

Adding the first integrals of the Euler equations that produce minimization of Eq. (2) with respect to $c(x)$ and $\eta(x)$ produces:

$$\frac{\kappa^2}{2} \left(\frac{dc}{dx} \right)^2 + \frac{\nu^2}{2} \left(\frac{d\eta}{dx} \right)^2 = \Delta f(c, \eta) \quad \text{for } x > 0. \quad (3)$$

The integration constant vanishes because dc/dx , $d\eta/dx$, and Δf vanish as $x \rightarrow \infty$.

As the only minimum of $\eta(x)$ is at $x = 0$ (i.e., η_{GB}), $d\eta/dx > 0$ holds for all $x > 0$, and so c can be treated as a function of η : $c(x) = c(\eta(x))$. With Eq. (3), it is possible to relate dx to $d\eta$, which permits a change of variable in Eq. (2):

$$F = s\Delta\theta g(\eta_{GB}) + 2 \int_{\eta_{GB}}^1 \sqrt{2\Delta f(c, \eta) \left[\nu^2 + \kappa^2 \left(\frac{dc}{d\eta} \right)^2 \right]} d\eta, \quad (4)$$

where the GB excess energy F remains to be minimized with respect to function $c(\eta)$, the GB crystallinity η_{GB} , and composition $c_{GB} \equiv c(x=0)$.

The extremal conditions derived from the vanishing first variations of Eq. (4) with respect to $c(\eta)$ with one fixed end point [$\eta = 1$, $c(\eta = 1) = c_\infty$] and a free point (η_{GB} , c_{GB}) produces a system of equations that $c(\eta)$, η_{GB} , and c_{GB} of an equilibrium GB must satisfy:

$$\frac{\partial P}{\partial c} - \frac{\partial}{\partial \eta} \frac{\partial P}{\partial \frac{dc}{d\eta}} = 0 \quad \left(P \equiv \sqrt{2\Delta f(\eta, c) \left[\nu^2 + \kappa^2 \frac{dc^2}{d\eta} \right]} \right), \quad (5)$$

$$c(\eta = 1) = c_\infty, \quad \left. \frac{dc}{d\eta} \right|_{\eta_{GB}} = 0, \quad (6)$$

$$\frac{s\Delta\theta}{2} g'(\eta_{GB}) = \sqrt{2\nu^2 \Delta f(\eta_{GB}, c_{GB})}. \quad (7)$$

A graphical method solves Eqs. (5)–(7). First, a family of solutions to Eqs. (5) and (6) alone can be obtained by numerical solution to the second-order ordinary differential equation [Eq. (5)] subject to boundary conditions Eqs. (6) for all $\eta_{GB} \in (0, 1)$ [illustrated by dashed curves

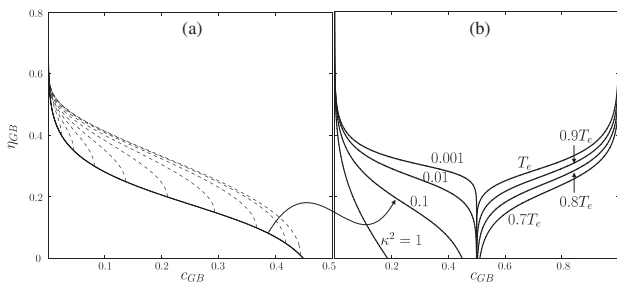


FIG. 1. (a) illustrates how \mathcal{C}_{PDE} (solid line) is obtained from solutions (dashed lines) to Eqs. (5) and (6). (b) Gradient coefficient and temperature dependence of \mathcal{C}_{PDE} . Because of A - B symmetry, two branches of curves are used to illustrate behavior: $T = 0.9T_e$ for the A -rich branch and $\kappa^2 = 0.01$ for the B -rich branch.

in Fig. 1(a) for nine distinct $\eta_{GB} \in (0, 1)$]. Let the curve \mathcal{C}_{PDE} be formed from the end points (η_{GB} , c_{GB}) of these solutions as illustrated by the continuous curve in Fig. 1(a); thus, \mathcal{C}_{PDE} reflects the dependence of GB composition on crystallinity as required by Eqs. (5) and (6). Next, solutions to Eq. (7) can be represented by a zero level set curve (\mathcal{C}_{LS}) in the $\eta - c$ plane. Finally, the equilibrium GB state, characterized by $(\eta_{GB}^{eq}, c_{GB}^{eq})$, satisfying Eqs. (5)–(7) is determined by the intersection of \mathcal{C}_{PDE} and \mathcal{C}_{LS} .

Curves \mathcal{C}_{PDE} and \mathcal{C}_{LS} were calculated for a modified regular solution model which produces a symmetric eutectic phase diagram [21]. To study the GBs in the A -rich phase within the two-solid-phase region, the matrix composition c_∞ was fixed at the temperature-dependent solubility limit of component A . As shown in \mathcal{C}_{PDE} in Fig. 1(b), c_{GB} tends towards the eutectic liquid composition $c_e = 0.5$ as η_{GB} decreases (because physically, Δf has smaller values near c_e for small values of η). Figure 1(b) illustrates that $c_{GB} \rightarrow c_e$ is also enhanced at higher temperatures and for smaller composition gradient coefficients κ .

For \mathcal{C}_{LS} [Eq. (7)], $\sqrt{2\nu^2 \Delta f}$ inherits its features from the Δf surface which has two global minima at solid A -rich and B -rich phases and one local minimum at the eutectic liquid state ($\eta = 0$, $c = c_e$) below the eutectic point T_e , as shown in Figs. 2(a) and 2(b). The $(s\Delta\theta/2)g'(\eta_{GB})$ plane is independent of c_{GB} and has a slope proportional to $\Delta\theta$. As illustrated in Fig. 2(a), $(s\Delta\theta/2)g'(\eta_{GB})$ intersects $\sqrt{2\nu^2 \Delta f}$

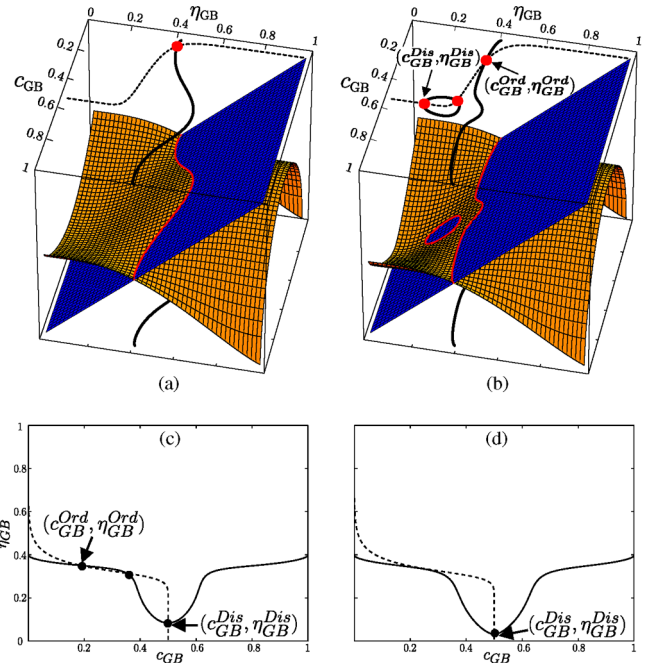


FIG. 2 (color online). Intersections between the $\sqrt{2\nu^2 \Delta f}$ and $(s\Delta\theta/2)g'$ surfaces produce \mathcal{C}_{LS} , which is highlighted by a thick line (also projected onto the top and bottom of the bounding box). Intersections between \mathcal{C}_{PDE} (dashed line) and \mathcal{C}_{LS} are highlighted by closed circle(s) at (a) $T = 0.9T_e$, (b) $0.99T_e$, (c) $0.995T_e$, and (d) $0.999T_e$. $\Delta\theta = 2.15$ and $\kappa^2 = 0.001$.

at relatively large η_{GB} values at large undercoolings ($T_e - T)/T_e$. Figure 2(a) shows that C_{PDE} and C_{LS} intersect only once, representing a relatively ordered GB with c_{GB}^{eq} close to c_∞ . As T increases towards T_e , the metastable liquid minimum of $\sqrt{2\nu^2\Delta f}$ decreases towards zero and approaches $(s\Delta\theta/2)g'(\eta_{GB})$ from above for small η_{GB} . For some values of material parameters and $\Delta\theta$, this results in the development of an isolated loop in C_{LS} close to the liquid state at small undercoolings, as illustrated in Fig. 2(b). Thus, two additional intersections of C_{PDE} and C_{LS} may be generated. The middle intersection shown in Fig. 2(b) corresponds to an unstable solution of Eqs. (5)–(7). The remaining two intersections are associated with two locally (meta)stable solutions. One solution $c^{Ord}(\eta)$, which also exists at lower temperatures [Fig. 2(a)], has a relatively ordered GB (η_{GB}^{Ord}) with low solute adsorption (c_{GB}^{Ord}). The other solution $c^{Dis}(\eta)$ represents a more disordered GB (η_{GB}^{Dis}) with larger adsorption (c_{GB}^{Dis}). $c^{Ord}(\eta)$ is the globally stable solution at lower temperatures, but $c^{Dis}(\eta)$ may become energetically favorable at small undercoolings. A first-order GB transition occurs when the two GB complexions have equal energy at a temperature T_{PM} , as shown in Fig. 3(a). Like η_{GB}^{eq} and c_{GB}^{eq} , the GB thickness has a discontinuous increase at T_{PM} [Fig. 3(a)].

Figure 2(c) shows that the two separate segments of C_{LS} may merge into a single curve at higher temperatures. As $T \rightarrow T_e$, the $(\eta_{GB}^{Ord}, c_{GB}^{Ord})$ solution and the unstable (middle) intersection may merge and disappear, as shown in Fig. 2(d), and leave the disordered GB as the only solution. $(\eta_{GB}^{Dis}, c_{GB}^{Dis})$ approaches $(0, c_e)$ as $T \rightarrow T_e$. Figure 3(a) shows that the GB energy reaches twice the solid-liquid interface energy and the GB thickness diverges at T_e . This suggests that the disordered GB is replaced at T_e by two solid-liquid interfaces with a layer of eutectic liquid of arbitrary thickness (i.e., the boundary is perfectly wet by the equilibrium liquid).

However, GB behavior near $T = T_e$ can possess at least two other modalities. For GBs with relatively small misorientations [e.g., $\Delta\theta = 1.2$ in Figs. 3(b) and 3(c)], the slope

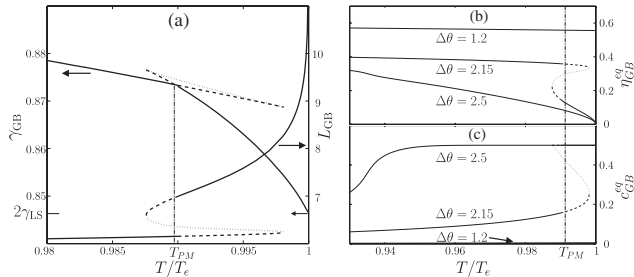


FIG. 3. (a) GB energy γ_{GB} and thickness L_{GB} vs T . L_{GB} is defined as the width of the region where $\eta < 0.99$. The GB transition temperature $T_{PM} = 0.9897$, and $\gamma_{LS} = 0.4233$ is the solid-liquid interface energy at T_e . (b)–(c) η_{GB}^{eq} and c_{GB}^{eq} vs T for $\Delta\theta = 2.5, 2.15$, and 1.2 . The dashed lines represent metastable extensions of ordered and disordered GBs, and the dotted lines are for the unstable solution.

of the $(s\Delta\theta/2)g'(\eta_{GB})$ plane in Fig. 2 is reduced and an isolated loop is not produced in C_{LS} . In this case, only a relatively ordered GB solution exists for $T < T_e$. The onset of perfect wetting may occur above T_e . At the other extreme, for GBs with relatively large misorientations [e.g., $\Delta\theta = 2.5$ in Figs. 3(b) and 3(c)], C_{LS} may be transformed from a high η_{GB} to a low η_{GB} region without the appearance of a loop and its multiple intersections with C_{PDE} . C_{LS} and C_{PDE} have only one intersection that moves continuously from $(\eta \approx 1, c \approx c_\infty)$ at low temperatures to $(0, c_e)$ as $T \rightarrow T_e$. In this case, no first-order transition occurs and the GB continuously disorders and increases its segregation until it perfectly wets at T_e .

The results shown in Figs. 1–3 are for average compositions in the two-phase region. The same analysis can be extended to the single-phase region by choosing a c_∞ that is smaller than the bulk solubility limit. For those $\Delta\theta$ which have a first-order GB transition in the two-phase region, multiple solutions can have limited persistence within the single-phase region above T_{PM} . The ordered-disordered GB coexistence line therefore extends into the single-phase region and may terminate at a critical point, as shown in Fig. 4. The disordered GB is the more stable structure between the coexistence line and bulk phase boundaries. When c_∞ approaches the solidus line from below at $T > T_e$, the disordered GB is wet by liquid as in the two-phase region for $T \rightarrow T_e$. This behavior is analogous to solute enrichment at a free surface as predicted by the critical point wetting model [22].

The predictions by our model analysis have been observed in various systems. Nanometer-thick, disordered Ni-rich GB layers were observed in high resolution TEM at subeutectic temperatures in 1%Ni-doped W [11]. In a Cu-Bi alloy, abrupt changes in GB segregation and crystallinity were observed in the Cu single-phase region, and

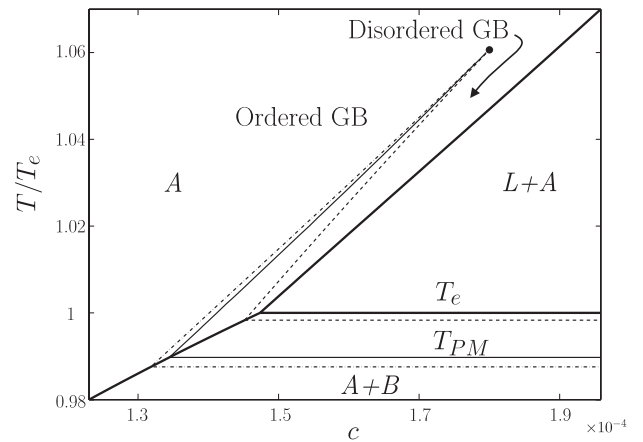


FIG. 4. Ordered/disordered GB coexistence line (thin solid line) in single-phase region for $\Delta\theta = 2.15$. The spinodal lines (i.e., limits of stability) of ordered GBs (dashed line) and disordered GBs (dashed-dotted line) are also shown. The coexistence line and the two spinodal lines terminate at a critical point ($T = 1.06T_e$, $c = 1.8 \times 10^{-4}$).

Bi-rich quasiliquid GBs were found to be stable close to the solidus line [12]. The “GB solidus line” drawn in Ref. [12] is analogous to the coexistence line in Fig. 4, but with the additional prediction of a critical point. Similar GB behavior was also observed in ceramic systems [e.g., ZnO-Bi₂O₃ [4] and Al₂O₃-(Y₂O₃ + SiO₂) [13]], known as intergranular glassy films (IGFs) that are apparently stable and have compositions that do not appear on the bulk equilibrium phase diagram. The general characteristics of IGFs (e.g., high segregation levels, large structural disorder, and equilibrium thickness) are consistent with the disordered GB complexion in our model. We suggest that IGFs are high-temperature equilibrium GBs from coupled premelting/prewetting transitions.

This crystallographic diffuse interface model [Eq. (1)] predicts that GB structural disordering and segregation cooperatively produce GB transitions below T_e . The predictions are consistent with experimental observations of GB premelting/prewetting phenomena. The model behavior depends on the solution thermodynamics of the material in question as well as gradient energy coefficients; however, the predicted behavior is sufficiently rich that it might fit many observations and thus may confound experimental verification or invalidation. Nevertheless, general behavior can be predicted. GBs with large misorientations are expected to undergo either first-order or continuous complexions transitions below the eutectic point in a two-phase region or within a single-phase region. Boundaries with smaller misorientations will remain ordered and unsegregated up to the solidus line or eutectic temperature. Macroscopic aspects of the observed compositions, structures, thicknesses, and stability of intergranular glassy films can be explained in the framework of grain boundary composition and structural transitions.

We are grateful for discussions with Jian Luo and Yet-Ming Chiang. As this manuscript neared completion, our coauthor R.M.C. died unexpectedly. W.C.C. and M.T. are grateful to him for many years of scientific discussion.

*Deceased.

- [1] J. W. Cahn, *J. Phys. (Paris)* **43**, 199 (1982).
- [2] K. E. Sickafus and S. L. Sass, *Acta Metall.* **35**, 69 (1987); D. Udler and D. N. Seidman, *Phys. Rev. Lett.* **77**, 3379 (1996); J. Creuze *et al.*, *Phys. Rev. Lett.* **86**, 5735 (2001).
- [3] B. Straumal and B. Baretzky, *Interface Sci.* **12**, 147 (2004); M. P. Seah, *J. Phys. F* **10**, 1043 (1980); P. L. Liu and J. K. Shang, *J. Mater. Res.* **16**, 1651 (2001).
- [4] H. F. Wang and Y.-M. Chiang, *J. Am. Ceram. Soc.* **81**, 89 (1998); J. Luo, H. F. Wang, and Y.-M. Chiang, *J. Am. Ceram. Soc.* **82**, 916 (1999).
- [5] C. Smith, in *Structure and Properties of Solid Surfaces* (University of Chicago, Chicago, 1952), p. 65; see also discussion by von Neumann, *ibid.*, p. 108.
- [6] R. Kikuchi and J. W. Cahn, *Phys. Rev. B* **21**, 1893 (1980); **36**, 418 (1987).
- [7] J. Q. Broughton and G. H. Gilmer, *Phys. Rev. Lett.* **56**, 2692 (1986); T. Nguyen *et al.*, *Phys. Rev. B* **46**, 6050 (1992); P. Keblinski *et al.*, *Phys. Rev. Lett.* **77**, 2965 (1996).
- [8] O. G. Mouritsen and M. J. Zuckermann, *Phys. Rev. Lett.* **58**, 389 (1987); G. Besold and O. G. Mouritsen, *Phys. Rev. B* **50**, 6573 (1994).
- [9] M. E. Glicksman and C. L. Vold, *Surf. Sci.* **31**, 50 (1972); E. L. Maksimova, L. S. Shvindlerman, and B. B. Straumal, *Acta Metall.* **36**, 1573 (1988).
- [10] A. Alsayed *et al.*, *Science* **309**, 1207 (2005).
- [11] J. Luo *et al.*, *Appl. Phys. Lett.* **87**, 231902 (2005).
- [12] L.-S. Chang *et al.*, *Acta Mater.* **47**, 4041 (1999); S. Divinski *et al.*, *Phys. Rev. B* **71**, 104104 (2005).
- [13] I. MacLaren *et al.*, *J. Am. Ceram. Soc.* **86**, 650 (2003).
- [14] R. Kobayashi, J. A. Warren, and W. C. Carter, *Physica (Amsterdam)* **140D**, 141 (2000); J. Warren *et al.*, *Acta Mater.* **51**, 6035 (2003).
- [15] M. Tang, W. C. Carter, and R. M. Cannon, *Phys. Rev. B* **73**, 024102 (2006).
- [16] Two- and three-dimensional versions are also available [14,17], but Eq. (1) suffices for planar GBs. In this case, $\Delta\theta$ can be interpreted as either a simple twist about the GB normal or tilt about a direction in the GB plane.
- [17] R. Kobayashi and J. A. Warren, *Physica (Amsterdam)* **356A**, 127 (2005).
- [18] The volume fraction of material affected by the GBs is assumed to be small enough so that c_∞ is a constant not affected by solute adsorption.
- [19] The form of $g(\eta)$ is subject to the physical constraints that it must be 0 if $\eta = 0$ (amorphous state) and monotonically increase with η . The effect of different $g(\eta)$ has been discussed in different contexts [14,15]. $g(\eta)$ used here is consistent with a single cusp at $\Delta\theta = 0$ in the GB energy— $\Delta\theta$ plot such as that in the Read-Shockley model. Multiple cusps, representing minima at low symmetry misorientations, could be introduced through modifying the prefactor sg as being $|\Delta\theta|$ -dependent.
- [20] R. Kobayashi and Y. Giga, *J. Stat. Phys.* **95**, 1187 (1999).
- [21] The model free energy is $f(c, \eta) = (1/\bar{v})\{f_A(\eta, T)(1 - c) + f_B(\eta, T)c + kT[c \ln c + (1 - c)\ln(1 - c)] + W(\eta) \times c(1 - c)\}$, where \bar{v} is the atomic volume. $f_A(\eta, T) = f_B(\eta, T) \equiv f^S(T) + a^2/2\eta^2(1 - \eta)^2 + \Delta H_m p(\eta) \times (T_m - T)/T_m$ are free energies of pure components per atom, where f^S is the free energy of the solid state. T_m and H_m are the melting temperature and enthalpy, respectively. The a^2 term in $f_{A,B}$ represents the energy barrier between solid and liquid states, and the function $p(\eta) = (1 - \eta)^3(1 + 3\eta + 6\eta^2)$ is a sigmoidal interpolation between $p(0) = 1$ and $p(1) = 0$. $W(\eta)$ is set to be $W_0 p(1 - \eta)$, making the interaction coefficient a decreasing function of η : The components are more miscible in the liquid phase. All variables and parameters are nondimensionalized as follows: Temperatures are scaled by T_m , energies by kT_m , lengths by $\bar{v}^{1/3}$, ν and κ by $a/\bar{v}^{1/6}$, and $\Delta\theta$ by $kT_m/(s\bar{v}^{2/3})$. In all calculations, $\Delta H_m = a^2 = 1.386$ and $W_0 = 5.883$ are chosen to produce a eutectic temperature $T_e = 2/3T_m$. ν is fixed at 1, which gives a solid-liquid interface thickness of about 4 atomic layers at T_e .
- [22] J. W. Cahn, *J. Chem. Phys.* **66**, 3667 (1977).